



Absolute radiotracer concentration measurement using whole-body solid-state SPECT/CT technology: in vivo/in vitro validation

John A. Kennedy^{1,2} · Ilya Reizberg¹ · Rachel Lugassi¹ · Shoham Himmelman¹ · Zohar Keidar^{1,2}

Received: 26 July 2018 / Accepted: 4 April 2019 / Published online: 25 April 2019
© International Federation for Medical and Biological Engineering 2019

Abstract

The accuracy of recently approved quantitative clinical software was determined by comparing in vivo/in vitro measurements for a solid-state cadmium-zinc-telluride SPECT/CT (single photon emission computed tomography/x-ray computed tomography) camera. Bone SPECT/CT, including the pelvic region in the field of view, was performed on 16 patients using technetium-99m methylene diphosphonic acid as a radiotracer. After imaging, urine samples from each patient provided for the measurement of in vitro radiopharmaceutical concentrations. From the SPECT/CT images, three users measured in vivo radiotracer concentration and standardized uptake value (SUV) for the bladder using quantitative software (Q.Metrix, GE Healthcare). Linear regression was used to validate any in vivo/in vitro identity relations (ideally slope = 1, intercept = 0), within a 95% confidence interval (CI). Thirteen in vivo/in vitro pairs were available for further analysis, after rejecting two as clinically irrelevant (SUVs > 100 g/mL) and one as an outlier (via Cook's distance calculations). All linear regressions ($R^2 \geq 0.85$, $P < 0.0001$) provided identity in vivo/in vitro relations (95% CI), with SUV averages from all users giving a slope of 0.99 ± 0.25 and intercept of 0.14 ± 5.15 g/mL. The average in vivo/in vitro residual difference was < 20%. Solid-state SPECT/CT imaging can reliably provide in vivo urinary bladder radiotracer concentrations within approximately 20% accuracy. This practical, non-invasive, in vivo quantitation method can potentially improve diagnosis and assessment of response to treatment.

Keywords SPECT/CT · Quantitation · Cadmium-zinc-telluride · CZT

1 Introduction

1.1 Background

Scintigraphy has been the standard diagnostic tool in nuclear medicine because of its high sensitivity in finding pathology. This medical imaging technique can reveal physiological changes related to pathology, often well before more subtle anatomical changes can be seen in x-ray radiographs or other imaging modalities. Scintigraphy is regularly being improved.

Historically, the visualization of the gamma camera was as a two-dimensional, flat, projection image of radiotracer

emissions, analogous to a simple x-ray radiograph. Whereas the high energy photons in x-ray imaging are generated external to the patient, scintigraphy provides a map of radiotracer concentration with γ -ray photons being emitted from within the patient via the radioactive decay of the radiotracer. By obtaining projection images from many angles around the patient, the tomographic technique provides three-dimensional (3-D) images by means of image reconstruction algorithms. As x-ray radiographs evolved into x-ray computed tomography (CT), so too the flat scintigraphic visualization evolved into 3-D single photon emission computed tomography (SPECT) [1–3].

The detailed volumetric imaging of radiopharmaceuticals has made SPECT an important diagnostic tool in fields such as orthopedics, oncology, cardiology, and nephrology, among others [4–7]. A major development in SPECT was its integration with CT by means of a fixed coaxial registration between SPECT and CT gantries, referred to as a hybrid SPECT/CT scanner [8, 9]. The added value of CT to SPECT has been proven clinically [10–13] by enabling the precise localization of radiotracer uptake with respect to anatomy and facilitating

✉ John A. Kennedy
j_kennedy@rambam.health.gov.il

¹ Department of Nuclear Medicine, Rambam Health Care Campus, P.O.B. 9602, 3109601 Haifa, Israel

² The Ruth & Bruce Rappaport Faculty of Medicine, Technion–Israel Institute of Technology, Haifa, Israel

the removal of artifacts which degrade the SPECT image through processes like γ -ray photon attenuation and scatter.

Regardless of continual technical advances, by a number of criteria SPECT/CT has not met the performance of positron emission tomography (PET)/CT. For example, SPECT continues to suffer from poorer photon detection efficiency (sensitivity) and spatial resolution than PET, giving images with comparatively more noise and blur. The limited image quality of SPECT compared with PET also limits the accuracy of SPECT radiotracer quantitation. However, SPECT has the benefit in some situations of longer radionuclide half-lives, which may better suit biological processes of interest, as well as the ability to perform multitracers studies using detector pulse height spectroscopy to separate different radiolabels emitting photons of different energies.

The use of absolute quantitative measurements of radiotracer concentrations is standard practice in clinical PET/CT and plays an important role in diagnosis, the evaluation of the patient's response to therapy, disease monitoring, and clinical evaluation. Conversely, quantitative analysis in SPECT/CT has not been a routine in the clinic due to technical limitations, significantly reducing the information content of this method. This has been the clinical reality even though historically SPECT imaging preceded PET imaging and quantitation methods were developed for SPECT before PET.

Quantitative SPECT/CT has the potential to greatly improve the clinical practice of modern nuclear medicine by reducing the subjective, user-dependent component of the visual interpretation of SPECT. There is a need for standard, quantitative, and more objective clinical metrics for image evaluation. Bailey and Willowson [14] have published an extensive list of potential uses of quantitative SPECT in a clinical setting which includes theranostics, treatment planning, measurement of monitoring response to treatment, assessing disease progression, measurement of coronary flow reserve, dynamic analysis of myocardial perfusion, and neurotransmitter brain imaging of receptor density and occupancy.

1.2 Literature review

Many methods have been developed to provide absolute radiotracer concentrations from SPECT images. For example, phantom studies have shown good quantitative SPECT measurements by judicious use of filtering on emission data coupled with attenuation correction and scatter estimation [15] or by simultaneously modeling attenuation, scatter, and collimator resolution effects [16]. Early development of a coaxial hybrid SPECT/CT device as a research tool [17] enabled absolute radiotracer concentration in the myocardium of a porcine model by using the CT to generate an attenuation map and provide data for partial volume correction [18], and CT data has been used to model scatter during image reconstruction [19].

Recently, advances in commercial multimodality camera hardware improved algorithms for image reconstruction, and clinically available sophisticated compensation techniques to correct for photon attenuation and scattering have made quantitative SPECT viable in practice. Clinical attempts to evaluate the normal and pathological distribution of the standardized uptake value (SUV) or absolute radioactivity concentration from quantitative bone SPECT and SPECT/CT has been described in the literature [20–22], but these methods are not widely available for practical application in the clinic.

1.3 Current study

A software package (Q.Metrix software, GE HealthCare) that allows quantitative measurement of radiotracer concentration within the body being scanned by SPECT/CT has recently been developed and become commercially available. The software has been approved for clinical use and has been installed on workstations at our site, and to date has not been clinically validated on a whole-body solid-state SPECT/CT camera.

The introduction with such software of an SUV index in SPECT has the potential to improve the diagnostic accuracy and the understanding of the disease. Our goal was to assess the accuracy of measuring the true concentration of the visualization agent, the radiopharmaceutical ^{99m}Tc -MDP (technetium-99 m methylene diphosphonic acid), in the human body via this software for a general purpose solid-state SPECT/CT.

2 Methods

2.1 Q.Metrix software package

The Q.Metrix software package is a commercially available tool designed to integrate acquisition data in order to facilitate quantitative measurements of SPECT data. As inputs, the software requires the SPECT and CT image data sets, patient weight, injected activity, time of injection, activity remaining in the used syringe along with the time of this measurement, and NEMA (National Electrical Manufacturers Association) system sensitivity values [23]. The SPECT images are required to be attenuation corrected and scatter corrected, both of which are done iteratively in the forward projection step of an ordered subset expectation maximization image reconstruction (OSEM) algorithm. The reconstruction uses resolution recovery which includes collimator modeling in the system matrix of OSEM. Selection tools on the Q.Metrix display enable the generation of volumes of interest (VOIs) on either the SPECT or CT images, which are coregistered. VOIs may be chosen by placing and sizing standard shapes, by region growing methods, or by thresholding methods. VOIs are automatically translated between modalities, but the quantitative

measurements reference SPECT values only, with no quantitative measurements made on CT.

As outputs, the software can provide maximum and average uptake values throughout a VOI in units of MBq/mL and standardized uptake value (SUV). As in PET quantitation, the standardized uptake value is the radiotracer concentration in MBq/mL normalized by the average radiotracer concentration in the patient at scan time:

$$\text{SUV} = \frac{\text{voxel concentration in MBq/mL}}{\text{decay corrected injected dose in MBq/patient mass in grams}}$$

where the patient mass in grams acts as a volume surrogate, replacing milliliters. The metric SUV has the property that regardless of scan time or injected dose, if the radiotracer is homogeneously distributed throughout the entire volume, and if the volume has the density of water, then the SUV value is 1 g/mL. Regions with higher radiotracer concentrations have higher SUVs.

2.2 Solid-state CZT SPECT/CT

A solid-state whole-body SPECT/CT camera employing CZT (cadmium-zinc-telluride) detectors was employed (Discovery 670, GE Healthcare, Tirat Carmel, Israel). The CZT module characteristics are described elsewhere [24], and in this configuration, a rectangular-hole lead collimator with a pitch of 2.46 mm × 2.46 mm, hole size of 2.26 mm × 2.26 mm, and hole length of 5 cm was used. The camera comprised dual flat panel detectors mounted on a rotating gantry and has a similar exterior appearance to standard dual-headed Anger SPECT clinical cameras. Each detector head consisted of 10 rows of 13 columns of CZT modules providing projection data covering 40 cm × 52 cm field of view (FOV). The SPECT gantry was coaxial with a 16-slice diagnostic CT gantry, with a shared patient handling bed.

2.3 Phantom study

SPECT image calibration for quantitative measurements was determined by a NEMA body phantom emulating clinical count rates and higher (1.2, 1.8, 3.7, 19, and 24 kcounts/s per detector) loaded with a “lung” insert and six hot spheres (10, 13, 17, 22, 28, and 37 mm in diameter) with a 12.1:1 target-to-background ratio (TBR) of $^{99\text{m}}\text{Tc}$ -pertechnetate solution (Fig. 1). Background concentrations were 5.4, 8.3, 16.8, 86, and 109 kBq/mL. The phantom acquisitions conformed to a bone SPECT protocol. Two detector heads were rotated 360° about the patient in H-mode (180° per head) every 6° giving 60 projections on a 128 × 128 matrix. The camera zoom was 1 and the time per projection was 30 s. Standard energy windows were used: 140 keV ± 10% for the emission counts and 120 keV ± 5% for the scatter counts used in scatter

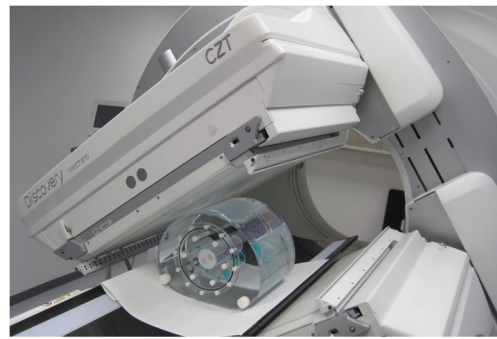


Fig. 1 SPECT image calibration was determined by a NEMA body phantom loaded with a “lung” insert and six hot spheres, using solid-state CZT detectors

correction. The SPECT acquisition was followed by a CT using 120 kV and a current of 80 mA. The CT provided a 2.5 mm slice thickness with a 512 × 512 matrix spanning a 50 cm FOV. SPECT images were reconstructed on an Xeleris 4.0 Workstation (GE Healthcare, Tirat Carmel, Israel) using OSEM with 10 subsets and 4 iterations with CT attenuation correction, scatter correction, and resolution recovery. For quantitative measurements, no pre- or post- image reconstruction filtering was performed. Using NEMA system sensitivity values [23] measured on the same camera employed for the clinical study, the scatter weight was adjusted until reconstructed SPECT image background values were 1 g/mL as measured on Q.Metrix. Hot sphere results using Method B, described below in Section 2.4.1, provided an estimate of expected variability in absolute quantitative SPECT measurements compared with the known concentration.

2.4 Clinical study

Sixteen patients referred for bone scintigraphy as part of their clinical assessment were included in a reference-controlled study (in vivo/in vitro) approved by the institutional ethics committee (#0201–16–RMB). The patient population consisted of 12 females and 4 males, without extreme weight or age characteristics (Table 1).

Volumetric imaging was according to a standard SPECT/CT hip imaging protocol spanning about 30 cm axially along the patient at the hip, approximately 2.5 h after a nominal injection of 925 MBq (25 mCi) $^{99\text{m}}\text{Tc}$ -MDP. The patients were not under fast, and during the uptake duration from injection to scan time, they were instructed to drink six to eight glasses of water. Acquisitions and image reconstructions followed the SPECT protocol given above in Section 2.3 except the durations were 17 s per projection. The SPECT acquisition was followed by a CT, as described above, except that the current ranged from 80 to 200 mA (varied automatically as per patient attenuation at each axial location). SPECT image calibration was determined by a body phantom as described above.

Table 1 Patient population demographics

Patient	Sex	Age (years)	Weight (kg)	Injected dose (MBq)	Uptake Duration (h)
1	F	80	60	857	2.63
2	F	38	62	1010	2.43
3	F	51	75	883	2.30
4	F	62	72	838	2.25
5	M	58	88	938	2.57
6	M	72	84	878	2.93
7	F	71	70	896	2.33
8	F	40	78	930	2.57
9	M	79	85	889	2.48
10	M	68	83	855	3.20
11	F	62	62	810	2.37
12	F	44	78	888	2.87
13	F	40	110	900	2.25
14	F	65	60	803	2.00
15	F	66	77	932	2.22
16	F	86	70	908	2.70
Average:		61	76	888	2.50
SD:*		15	13	51	0.31

*SD standard deviation

2.4.1 In vivo study

Data relevant to the average absolute concentration of the radiotracer in the bladder were collected by three users with Q.Metrix

Software using an Xeleris 4.0 Workstation (GE Healthcare, Tirat Carmel, Israel). The users were a senior physician with 5 years' experience in reading clinical nuclear studies, a senior physicist with 16 years' experience researching nuclear medicine processes, and a junior physicist with 5 months' experience viewing nuclear medicine images (users A, B, and C, respectively). They each employed slightly different methods to make the quantitative measurements, referred to here as methods A, B, and C, respectively. In method A, clinical experience was used to subjectively estimate the edge of the bladder in the SPECT image to establish the volume of interest (VOI) for measurement. For method B, the VOI was determined by a threshold set at 42% of the maximum uptake found within the bladder (Fig. 2), consistent with methods for finding metabolic tumor volume in PET [25]. In method C, the user was instructed to draw a sphere of maximum size within the region of uptake of the bladder as visualized on the SPECT images. In all methods, the boundary was cross checked with coregistered CT views provided by the software to ensure that it was within the anatomical view of the bladder, and users were instructed to alter the boundary to fit the anatomical view of the bladder if necessary. These absolute in vivo radiotracer concentration measurements using Q.Metrix were compared with in vitro urine sample measurements as detailed in the next section.

2.4.2 In vitro study

Immediately after the SPECT scan, the patient was requested to provide a urine sample. Approximately 8 mL of urine was drawn

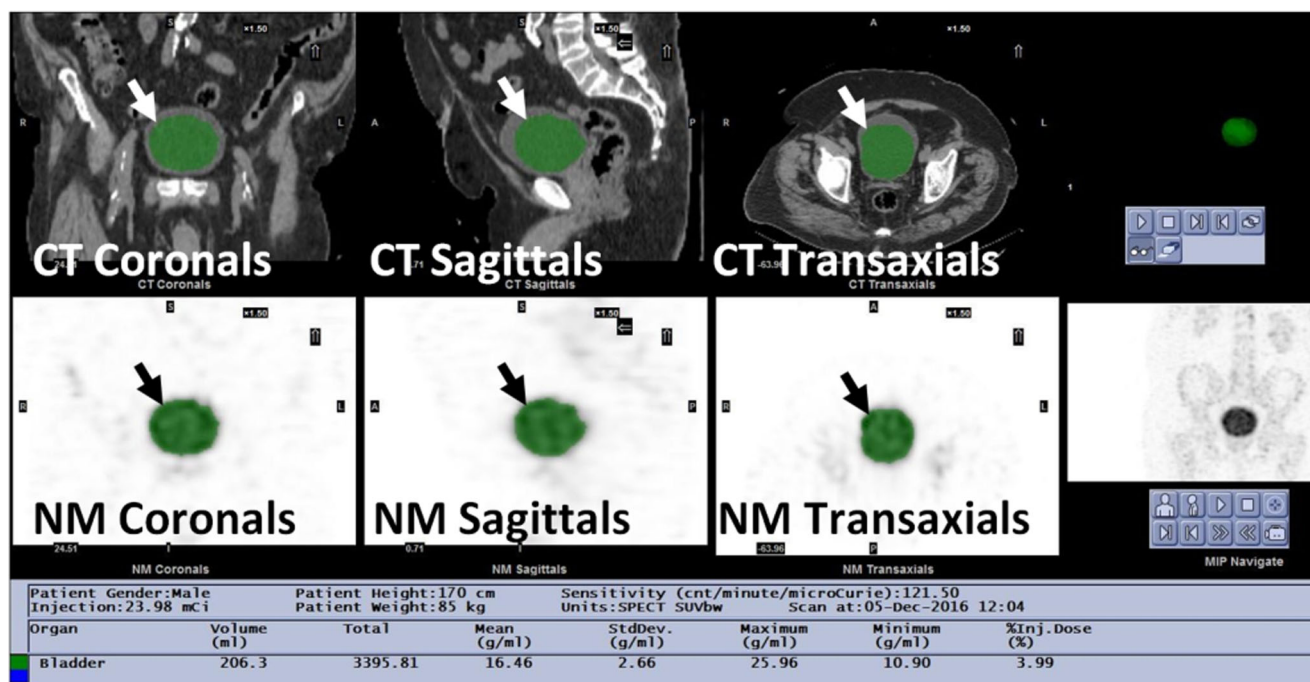
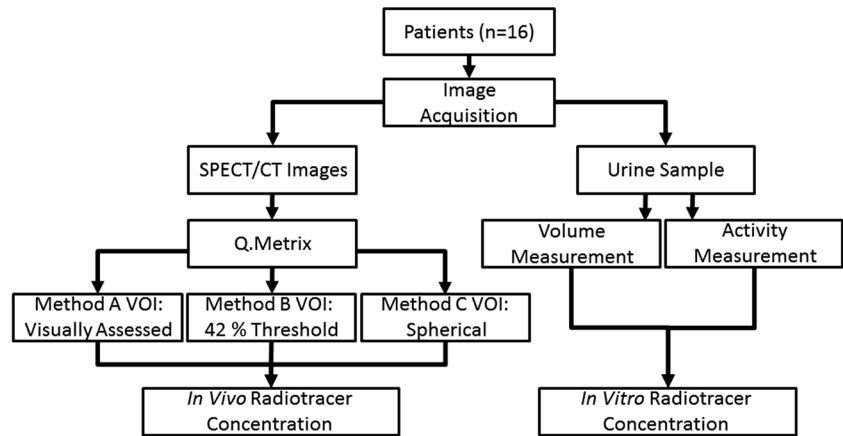


Fig. 2 Screen shot of the software output for patient 5, Method B. VOI of bladder (arrows) was determined by contiguous voxels within the bladder radiotracer uptake that fall above 42% of the maximum uptake within the bladder. CT fused images (upper row) confirm localization to the bladder

Fig. 3 Schematic of the clinical study method for in vivo/in vitro measurements



from an approximately 100 mL sample into a standard 10-mL urine sample tube. The activity in this tube was measured in a calibrated dose calibrator (Model CRC25, Capintec, Inc., Florham Park, NJ) and the precise volume determined by net weight in grams assuming a density of 1 g/mL. Radiotracer concentration was calculated and decay corrected to scan time for comparison with quantitative SPECT measurements.

Figure 3 shows a schematic of the in vivo/in vitro methods for the clinical study. Linear regression was used to establish a relationship, if any, between in vivo bladder SUV measurements made with Q.Metrix and in vitro urine concentrations which had also been normalized to SUV values. Data related to urine concentrations with effective SUVs greater than 100 g/mL were not included in the linear regression since such values are not clinically relevant to ^{99m}Tc-MDP bone scans. Outliers were identified using Cook’s distance with a threshold of three times the mean Cook’s distance for the regression [26, 27], and dropped after this identification if there was an obvious mismatch such as an order of magnitude difference among measured values. Similar analyses were performed on decay corrected activity concentrations in units of MBq/mL, without the SUV normalization.

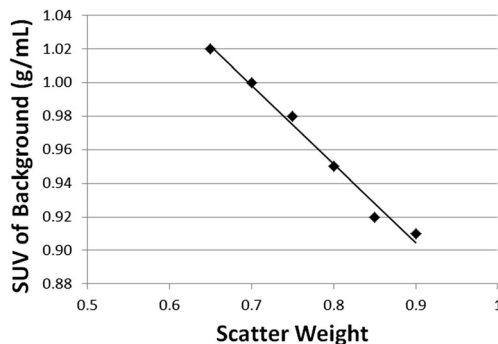


Fig. 4 SUV of background vs. scatter weight: Phantom SPECT calibration shows that a scatter weight of 0.70 sets the background SUV intensity in the image at the known value of 1.0 g/mL. A linear regression line of best fit (slope = 0.469, intercept = 1.327, $R^2 = 0.987$) supports this choice

3 Results

3.1 Phantom measurements

System sensitivity was 54.7 counts/s/MBq on average for each detector according to NEMA methods. Using the highest count phantom results (109 kBq/mL) with the least noise, a scatter weight of 0.70 set the background SUV intensity in the SPECT reconstructed images at the known value of 1.0 g/mL, as measured by Q.Metrix (Fig. 4). Among the three largest spheres (volumes from 5.6 to 26.5 mL) and five different concentrations, variability from the expected 12.1:1 TBR ranged from 6.6 to 22.7% with an average of 14.0%, with all values biased negatively.

3.2 Clinical measurements

Uptake duration was 2.5 ± 0.3 h (mean \pm standard deviation) ranging from 2.0 to 3.2 h (Table 1). The injected dose was 888 ± 51 MBq. Volume measurements of the VOI on Q.Metrix ranged from 1.3 to 321 mL, encompassing from 15 to 3718 voxels. Patients 15 and 16 had urine concentrations with effective SUVs greater than 100 g/mL (Table 2) so they were not included in the linear regression since such values are not clinically relevant to ^{99m}Tc-MDP bone scans. For all three methods, results from patient 14 were indicated as possible outliers since the Cook’s distances were > 2.3 , which is above a threshold of three times the mean Cook’s distance for each linear regression of SPECT concentration vs. urine concentration measurements. Investigation showed that there is an order of magnitude difference among the three methods (Table 2), so this in vivo/in vitro pair was not used in the linear fitting of the data. Linear regression of the in vivo vs. in vitro measurements of SUV and radiotracer concentration in MBq/mL provided slopes of 1 and intercepts of 0 for all three methods, within the 95% confidence intervals (Table 3), as depicted in Fig. 5. For the linear fits, the average of

Table 2 Decay corrected measurements of in vitro urine samples and in vivo SPECT imaging

Patient	SUV (g/mL)			Concentration (MBq/mL)				
	In vitro	In vivo SPECT method			In vitro	In vivo SPECT method		
		A	B	C		A	B	C
1	13.2	16.6	15.3	16.3	0.119	0.150	0.138	0.147
2	17.0	22.3	20.9	21.9	0.152	0.200	0.187	0.196
3	19.1	15.3	21.0	20.2	0.186	0.150	0.204	0.197
4	10.3	9.1	8.1	6.9	0.091	0.080	0.071	0.061
5	14.4	19.2	16.5	11.5	0.113	0.150	0.129	0.132
6	11.7	10.2	6.5	6.7	0.085	0.074	0.047	0.048
7	13.1	15.1	13.4	13.0	0.130	0.150	0.133	0.129
8	7.8	7.4	7.2	6.2	0.064	0.060	0.059	0.051
9	7.8	9.5	10.0	8.8	0.049	0.060	0.063	0.056
10	15.0	17.9	17.0	16.3	0.159	0.190	0.181	0.173
11	7.3	8.6	8.8	9.1	0.068	0.080	0.082	0.085
12	52.2	66.6	55.5	51.6	0.494	0.630	0.526	0.488
13	33.0	21.9	18.9	20.0	0.347	0.230	0.199	0.210
14	36.6	89.7	5.4	5.0	0.449	1.100	0.066	0.061
15	163.5	111.4	84.6	78.9	1.291	0.880	0.668	0.624
16	145.6	103.8	85.6	92.8	1.080	0.770	0.636	0.690

the results of methods A, B, and C gave slopes nearest to unity, intercepts nearest to zero, and R^2 values (coefficient of determination) closer to unity, compared with any individual method (Table 3), with all p values less than 0.0001. A plurality of the points had residuals within 20% of the fitted average results: 8 of 13 points for the SUV plot and 9 of 13 points for the concentration plot; with the average residuals being within 18%.

4 Discussion

Data variability in SPECT imaging is the result of limited spatial resolution and noise introduced by Poisson counting statistics in radioactivity decay and detection processes [28]. Due to partial volume effects, the former artifactually reduces voxel values within small volumes of uptake, or at the edges of uptake. The latter results in artefactual inhomogeneities as

Table 3 Linear regression parameters for in vivo SPECT vs. in vitro sample measurements

Parameter	Method			Average
	A	B	C	
SUV:				
Slope	1.145	0.941	0.896	0.994
CI* slope	−0.852 → 1.439	−0.687 → 1.195	−0.666 → 1.126	−0.748 → 1.241
Intercept (g/mL)	−1.102	0.785	0.744	0.143
CI intercept	−7.22 → 5.02	−4.52 → 6.09	−4.05 → 5.54	−5.00 → 5.29
R^2	0.870	0.858	0.870	0.877
Concentration:				
Slope	1.096	0.914	0.864	0.958
CI Slope	−0.807 → 1.385	−0.669 → 1.159	−0.646 → 1.083	−0.716 → 1.201
Intercept (MBq/mL)	−0.004	0.011	0.015	0.007
CI Intercept	−0.062 → 0.054	−0.038 → 0.060	−0.028 → 0.059	−0.041 → 0.055
R^2	0.863	0.859	0.873	0.873

*CI: 95% confidence interval

can be observed in Fig. 2 where the uptake within the bladder looks variable, but ^{99m}Tc -MDP in solution with urine is expected to be homogenous. Because of these limitations, it is expected that different users would collect slightly different absolute quantitation data from SPECT imaging especially when using different methods. Table 2 shows this variability between users although there is an overall concordance of the measurements: the line of best fit for the results of each user establishes an identity relation (slope = 1, intercept = 0) between *in vivo* and *in vitro* measurements (Table 3). Averaging the three methods likely reduces the effect of possible biases with each user and gives better overall agreement between the *in vivo* and *in vitro* tasks (Table 3). Taking the average line of best fit as a model of the true relationship between the *in vivo* SPECT measurements and the *in vitro* urine measurements, absolute SPECT quantitation was performed, for the most part, within a 20% accuracy, as indicated by the residuals to the fit. This is comparable with deviations of up to 17% reported using in-house methods and a standard SPECT system [29], even though the concentrations in the present study with the solid-state CZT camera was much higher (mean 0.158 MBq/mL, max. 0.494 MBq/mL) than that reported for the standard camera (mean 0.069 MBq/mL, max. 0.273 MBq/mL). As a rule, CZT detectors continue to respond linearly at high count rates, whereas standard cameras do not [24].

Compared with quantitative PET, some bone SPECT parameters facilitate more accurate measurement. The relative synchronization between the dose calibrator and the scanner would introduce an error of only 0.2% for every minute mismatch for ^{99m}Tc , compared with 0.6% for the isotope fluorine-18 often used in PET, due to the longer half-life of ^{99m}Tc . However, most other parameters work against quantitative SPECT accuracy compared with PET. Clinical SPECT spatial resolution is generally worse at 5–20 mm FWHM (full width at half maximum) for distances of 5 to 25 cm, compared with a typical value of 6 mm FWHM for clinical PET [30]. The sensitivity of PET is generally better, giving typical total counts of > 10 Mcounts for one tomographic FOV, compared with about 3 Mcounts for the SPECT studies presented here, enabling less statistical noise for PET. Regardless of these advantages, quantitative variability in PET due to physical factors can range up to 55% [31] and has been shown to be able to be reduced to 23% [32] or even 10% [33] among different scanners at different sites in multi-center trials, given sufficient care. This concurs with another PET quantitation study [34]. Typically, PET employs the maximum voxel measurement to reduce partial volume effects which makes the measurement more variable due to noise, although the variability can be reduced when some averaging techniques were applied. In the present study, by choosing a comparatively large feature with expected homogenous uptake, the urine in the bladder, the effect of voxel variability was reduced by

volumetric averaging. Regardless, the SPECT trial presented here, even with a variability of 20%, compares favorably with quantitative PET. Table 4 lists a comparison of absolute quantitation accuracy with illustrative studies.

In the interest of not misrepresenting this scanner, in this early configuration of the camera, the collimator hole length was 50 mm and the CZT crystal thickness was 5 mm, so the system sensitivity was lower than would be measured on the

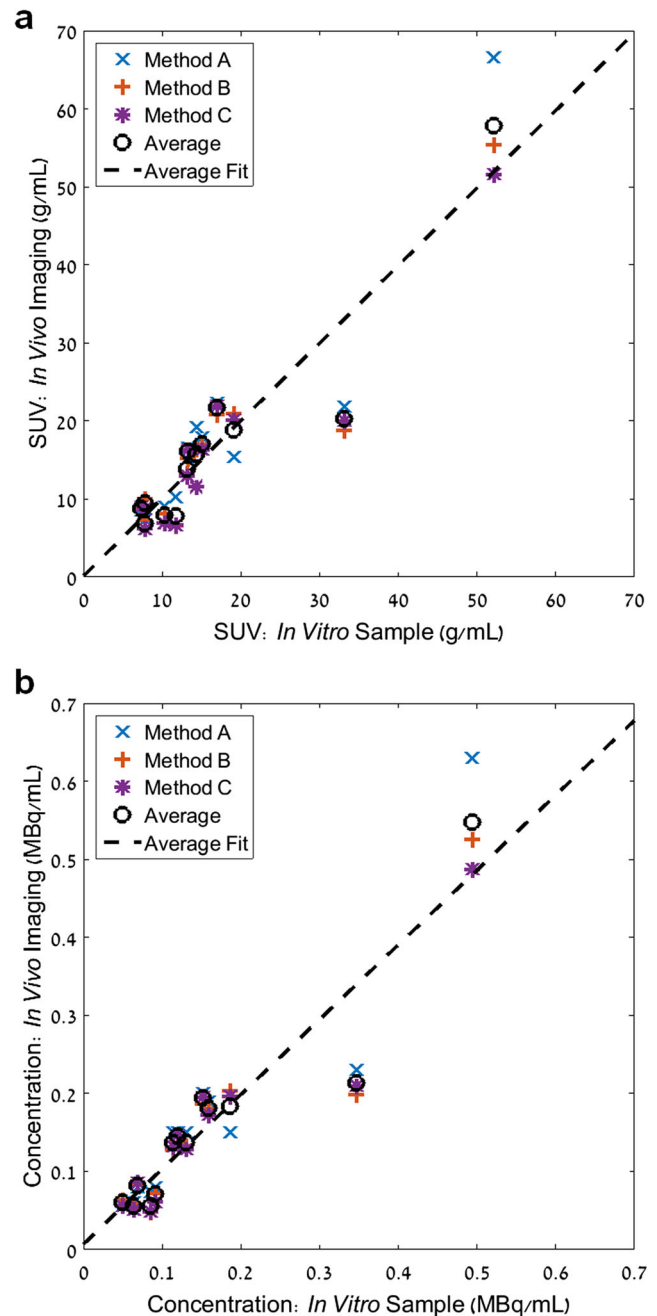


Fig. 5 In vivo SPECT results vs. in vitro urine sample results for SUV (a) and radiotracer concentration (b) measurements. Slopes of the average results (dashed line) were 0.99 and 0.96 with R^2 values of 0.88 and 0.87, respectively (Table 3)

Table 4 Comparison of absolute quantitation accuracy with illustrative studies

Study	Year	System	Emission source	Approximate reported accuracy
King et al. [15]*	1990	Clinical Anger camera	Phantom	20%
Walrand et al. [16]	1994	Clinical Anger camera	Phantom	5%
Da Silva et al. [18]	2001	Research Anger system	Porcine model	10%
Vandervoort et al. [19]	2007	Clinical Anger camera	Phantom	4%
Takahashi et al. [32]	2008	Multi-center PET	Phantom	23%
Boellaard et al. [33]	2008	Multi-center PET	Phantom	10%
Zeintl et al. [29]	2010	Clinical Anger camera	Patients	17%
Present study	2018	Clinical CZT camera	Patients	20%

*Superscript numbers refer to reference list

current commercial version: collimator hole length of 45 mm and CZT crystal thickness of 7.25 mm. The scatter weight of 0.7 should not be presumed to apply to different configurations and in practice, it is wise to calibrate each camera. The manufacturer's default scatter weight for the sodium-iodide crystal detector version of this camera is 1.1 for ^{99m}Tc radio-tracers, which is considerably higher than the value used here. This is because incomplete charge collection exacerbated by inhomogeneous electric fields across the crystal will assign more artefactual counts into the scatter energy window. Consequently, the weighting of these counts in scatter correction needs to be less. A thicker crystal is expected to reduce these inhomogeneities and lower the rate of incomplete charge collection which in turn should move the required scatter weight closer to unity. The concentrations of the three largest spheres of the phantom SPECT study here varied from the expected 12.1:1 TBR by approximately 14% which was comparable with the approximately 20% variability of the in vivo/ in vitro clinical measurements. Because the concentrations and geometry of the phantom were static, as opposed to the dynamic anatomy and physiology of the patient, the better accuracy from such phantom studies found here is to be expected.

5 Conclusions

Radiotracer concentrations in the urinary bladder can be reliably measured in vivo using a solid-state SPECT/CT camera to an accuracy of approximately 20%. This practical, non-invasive, in vivo quantitation method can potentially improve diagnosis and assessment of response to treatment.

Ethical approval All procedures performed in studies involving human participants were in accordance with the ethical standards of the institutional and/or national research committee and with the 1964 Helsinki declaration and its later amendments or comparable ethical standards.

References

- Jaszczak RJ (2006) The early years of single photon emission computed tomography (SPECT): an anthology of selected reminiscences. *Phys Med Biol* 51(13):R99–R115
- Moses WW, Gayshan V, Gektin A (2006) The evolution of SPECT—from Anger to today and beyond. In: Tavernier S, Gektin A, Grinyov B, Moses WW (eds) *Radiation detectors for medical applications*. Springer, Dordrecht, pp 37–80
- Jaszczak RJ, Coleman RE, Lim CB (1980) SPECT: Single photon emission computed tomography. *IEEE Trans Nucl Sci* 27(3):1137–1153
- Camargo EE (2001) Brain SPECT in neurology and psychiatry. *J Nucl Med* 42(4):611–623
- Madsen MT (2007) Recent advances in SPECT imaging. *J Nucl Med* 48(4):661–673
- Chowdhury FU, Scarsbrook AF (2008) The role of hybrid SPECT-CT in oncology: current and emerging clinical applications. *Clin Radiol* 63(3):241–251
- Germano G, Berman DS (2008) *Clinical gated cardiac SPECT*. Wiley, New York
- Schillaci O (2005) Hybrid SPECT/CT: a new era for SPECT imaging? *Eur J Nucl Med Mol Imaging* 32(5):521–524
- Mariani G, Bruselli L, Kuwert T et al (2010) A review on the clinical uses of SPECT/CT. *Eur J Nucl Med Mol Imaging* 37(10):1959–1985
- Bockisch A, Freudenberg LS, Schmidt D, Kuwert T (2009) Hybrid imaging by SPECT/CT and PET/CT: proven outcomes in cancer imaging. *Semin Nucl Med* 39(4):276–289
- Na CJ, Kim J, Choi S et al (2015) The clinical value of hybrid sentinel lymphoscintigraphy to predict metastatic sentinel lymph nodes in breast cancer. *Nucl Med Mol Imaging* 49(1):26–32
- Seo HJ, Ryu YH, Lee I et al (2015) Usefulness of (131)I-SPECT/CT and (18)F-FDG PET/CT in evaluating successful (131)I and retinoic acid combined therapy in a patient with metastatic struma ovarii. *Nucl Med Mol Imaging* 49(1):52–56
- Suh M, Cheon GJ, Seo HJ, Kim HH, Lee DS (2015) Usefulness of additional SPECT/CT identifying lymphatico-renal shunt in a patient with chyluria. *Nucl Med Mol Imaging* 49(1):61–64
- Bailey DL, Willowson KP (2013) An evidence-based review of quantitative SPECT imaging and potential clinical applications. *J Nucl Med* 54:83–89
- King MA, Coleman M, Penney BC, Glick SJ (1991) Activity quantitation in SPECT: a study of prereconstruction Metz filtering and the use of the scatter degradation factor. *Med Phys* 18:184–189

16. Walrand SHM, van Elmbt LR, Pauwels S (1994) Quantitation in SPECT using an effective model of the scattering. *Phys Med Biol* 39:719–734
17. Blankespoor SC, Wu X, Kalki K et al (1996) Attenuation correction of SPECT using x-ray CT on an emission-transmission CT system: myocardial perfusion assessment. *IEEE Trans Nucl Sci* 43:2263–2274
18. Da Silva AJ, Tang HR, Wong KH et al (2001) Absolute quantification of regional myocardial uptake of ^{99m}Tc -sestamibi with SPECT: experimental validation in a porcine model. *J Nucl Med* 42:772–779
19. Vandervoort E, Celler A, Harrop R (2007) Implementation of an iterative scatter correction, the influence of attenuation map quality and their effect on absolute quantitation in SPECT. *Phys Med Biol* 52:1527–1545
20. Israel O, Front D, Hardoff R et al (1991) In vivo SPECT quantitation of bone metabolism in hyperparathyroidism and thyrotoxicosis. *J Nucl Med* 32:1157–1161
21. Israel O, Keidar Z, Rubinov R, Iosilevski G, Frenkel A, Kuten A, Betman L, Kolodny GM, Yarnitsky D, Front D (2000) Quantitative bone single-photon emission computed tomography for prediction of pain relief in metastatic bone disease treated with rhenium-186 etidronate. *J Clin Oncol* 18:2747–2754
22. Kim J, Lee HH, Kang Y, Kim TK, Lee SW, So Y, Lee WW (2017) Maximum standardised uptake value of quantitative bone SPECT/CT in patients with medial compartment osteoarthritis of the knee. *Clin Radiol* 72(7):580–589
23. National Electrical Manufacturers Association (2012) Performance measurements of gamma cameras: NEMA standards publication NU 1–2012. NEMA, Rosslyn
24. Bocher M, Blevis IM, Tsukerman L, Shrem Y, Kovalski G, Volokh L (2010) A fast cardiac gamma camera with dynamic SPECT capabilities: design, system validation and future potential. *Eur J Nucl Med Mol Imaging* 37:1887–1902
25. Hatt M, Le Rest CC, Albarghach N, Pradier O, Visvikis D (2011) PET functional volume delineation: a robustness and repeatability study. *Eur J Nucl Med Mol Imaging* 38(4):663–672
26. Bollen KA, Jackman RW (1990) Regression diagnostics: an expository treatment of outliers and influential cases. In: Fox J, Long JS (eds) *Modern methods of data analysis*. Sage, Newbury Park, pp 257–291
27. MATLAB and Statistics Toolbox Release 2015b (2015) The MathWorks, Inc., Natick, Massachusetts, United States
28. Cherry SR, Sorenson JA, Phelps ME (2012) *Physics in nuclear medicine*, fourth edition. Elsevier, Philadelphia PA
29. Zeintl J, Vija AH, Yahil A, Hornegger J, Kuwert T (2010) Quantitative accuracy of clinical ^{99m}Tc SPECT/CT using ordered-subset expectation maximization with 3-dimensional resolution recovery, attenuation, and scatter correction. *J Nucl Med* 51:921–928
30. Meikle S, Kyme AZ, Kench P, Boisson F, Parmar A (2017) Preclinical PET and SPECT. In: Dahlbom M (ed) *Physics of PET and SPECT imaging*. CRC press. Taylor & Francis Group, New York, pp 413–438
31. Boellaard R (2009) Standards for PET image acquisition and quantitative data analysis. *J Nucl Med* 50:11S–20S
32. Takahashi Y, Oriuchi N, Otake H et al (2008) Variability of lesion detectability and standardized uptake value according to the acquisition procedure and reconstruction among five PET scanners. *Ann Nucl Med* 22:543–548
33. Boellaard R, Oyen WJG, Hoekstra CJ et al (2008) The Netherlands protocol for standardisation and quantification of FDG whole body PET studies in multi-centre trials. *Eur J Nucl Med Mol Imaging* 35: 2320–2333
34. Lodge MA, Chaudhry MA, Wahl RL (2012) Noise considerations for PET quantification using maximum and peak standardized uptake value. *J Nucl Med* 53:1041–1047

Publisher's note Springer Nature remains neutral with regard to jurisdictional claims in published maps and institutional affiliations.



John A. Kennedy is a physicist at Rambam Health Care Campus and an adjunct lecturer in biomedical engineering at the Technion, Israel. He has a number of publications on SPECT and PET imaging.



Ilya Reizberg performed this study as a senior physician of the Department of Nuclear Medicine at Rambam Health Care Campus. He has published research on the topic of nuclear cardiology.



Rachel Lugassi is a physicist for the Department of Nuclear Medicine, Rambam Health Care Campus. She has research published on the topic of radiation safety in nuclear medicine.



Shoham Himmelman is a junior physicist for the Department of Nuclear Medicine, Rambam Health Care Campus, and a graduate of the Faculty of Physics, Technion–Israel Institute of Technology, Haifa, Israel.



Zohar Keidar is the director of the Department of Nuclear Medicine at Rambam Health Care Campus and a clinical professor at the Technion, with internationally recognized nuclear medicine research.